

Noise suppression of time-migrated gathers using prestack structure-oriented filtering

Bo Zhang¹, Tengfei Lin², Shiguang Guo², Oswaldo E. Davogustto², and Kurt J. Marfurt²

Abstract

Prestack seismic analysis provides information on rock properties, lithology, fluid content, and the orientation and intensity of anisotropy. However, such analysis demands high-quality seismic data. Unfortunately, noise is always present in seismic data even after careful processing. Noise in the prestack gathers may not only contaminate the seismic image, thereby lowering the quality of seismic interpretation, but it may also bias the seismic prestack inversion for rock properties, such as acoustic- and shear-impedance estimation. Common postmigration data conditioning includes running window median and Radon filters that are applied to the flattened common reflection point gathers. We have combined filters across the offset and azimuth with edge-preserving filters along the structure to construct a true “5D” filter that preserves amplitude, thereby preconditioning the data for subsequent quantitative analysis. We have evaluated our workflow by applying it to a prestack seismic volume acquired over the Fort Worth Basin, TX. The inverted results from the noise-suppressed prestack gathers are more laterally continuous and have higher correlation with well logs when compared with those inverted from conventional time-migrated gathers.

Introduction

During the past decade, poststack structure-oriented, edge-preserving filtering has led to improved data continuity, providing sharper fault edges and the improved performance of automated picking. Such poststack migrated seismic data can provide an excellent image of the subsurface structure and stratigraphy. More quantitative interpretation products, such as simultaneous prestack inversion, provide estimation of acoustic impedance (Z_P), shear impedance (Z_S), and density, whereas prestack amplitude variation with azimuth (AVAz) analysis provides measures of the orientation and strength of subsurface anisotropy. The quality of the estimated properties is highly dependent on the data quality of prestack seismic data. Because stacking is in itself a filter, it is obvious that noise that contaminates poststack data is equal or stronger on prestack seismic gathers. Undesired prestack seismic phenomena need to be diminished or removed prior to reservoir characterization (Singleton, 2008). Although there has been considerable work on residual velocity analysis and trim statics, most publications that address the reduction of crosscutting noise on seismic gathers have been limited to processing across offset, one gather at a time.

Structure-oriented filtering is one of the most popular processes to improve the quality of the poststack

seismic image. Bilateral filters were initially used for smoothing photographic images, while preserving edges (Tomasi and Manduchi, 1998). However, bilateral filters cannot be applied directly to seismic images because seismic edges differ significantly from those in photographic images (Hale, 2011). Weickert (1999) enhances the continuity of coherent reflections, while preserving lateral discontinuities, such as chaotic structures and faults using an anisotropic diffusion filter. Luo et al. (2002) use a multiwindow Kuwahara filter to achieve the same purpose, for which they compute the mean and variance in a suite of overlapping windows containing the same analysis point. The output is then set to the mean of the window having the smallest variance. Fehmers and Höcker (2003) compute structural dip and chaos (a coherence like measure) using the gradient structure tensor. If the chaos is below a threshold, the data are smoothed “anisotropically” along the structure, whereas if the chaos is large, such as about a fault, the data are left unchanged. AlBinHassan et al. (2006) improve Luo et al.’s (2002) algorithm by using 3D one-sided and centered smoothing operators. Marfurt (2006) builds on the Kuwahara concept by using coherence rather than variance to choose the most coherent window, followed by increasing the statistical leverage against noise by applying a 3D Karhunen-Loève (KL)

¹The University of Alabama, Department of Geological Sciences, Tuscaloosa, Alabama, USA. E-mail: bzhang33@ua.edu.

²The University of Oklahoma, ConocoPhillips School of Geology and Geophysics, Norman, Oklahoma, USA. E-mail: tengfei.lin@ou.edu; beiergo@ou.edu; dellpi@me.com; kmarfurt@ou.edu.

Manuscript received by the Editor 21 August 2015; published online 21 March 2016. This paper appears in *Interpretation*, Vol. 4, No. 2 (May 2016); p. SG19–SG29, 12 FIGS.

<http://dx.doi.org/10.1190/INT-2015-0146.1>. © 2016 Society of Exploration Geophysicists and American Association of Petroleum Geologists. All rights reserved.

(principal component) filter to the data along the structural dip. Whitcombe et al. (2008) and Helmore (2009) introduce frequency dependent, structure-oriented filters. Wang et al. (2009) also notice that the local reflector dip depends on the frequency band of the seismic data and suppress the seismic noise using a suite of band-pass structure-oriented filters. Liu et al. (2010) reduce random noise, while protecting structural information by combining structural prediction with either mean filtering or lower-upper median (LUM) filtering, using plane-wave destruction filters to estimate the reflector dip. Corrao et al. (2011) also use structure-oriented LUM filters, and show how it provided greater control of noise rejection over the more commonly used mean and median filters. Hale

(2011) applies bilateral filters to perform edge-preserving smoothing for seismic images by replacing the domain kernel of a bilateral filter with a smoothing filter. Like Fehmers and Höcker (2003), the anisotropic smoothing filter is based on the gradient structure tensor.

The traditional way of removing random noise with a Gaussian distribution is to stack the data (Hendrickson, 1999). However, prestack analysis requires prestack seismic gathers or angle-limited stacked gathers. Prestack noise suppression is an important but inadequately solved problem in seismic processing. It is important for improving amplitude variation with offset (AVO) and AVAZ analysis. Castagna and Backus (1993) show that noise in the prestack gathers could bias or corrupt the reflectivity variation with offset. Cambois (1998) states that background trends observed from AVO crossplots can be an indicator of rock properties or a noise trend. Hendrickson (1999) notices that AVO crossplot from Auger Field and the crossplot from random noise share similar features, which indicate that the observed background AVO trend can be just noise. Cambois (2000) further finds that noise in the P-wave seismic data may change the form of wavelet variation with offset and bias the estimation of rock properties. Simm et al. (2000) find that random noise can be a significant component of noise on AVO crossplots. Buland and Omre (2003a, 2003b) find that AVO inversion and the wavelet estimation depend on the noise covariance. Koza and Castagna (2003) conclude that random noise may rotate the trend of AVO crossplots and obscure the petrophysics properties. They tried to remove the noise to which Radon filters are applied. Hennenfent and Herrmann (2004) present a method to stabilize the three-term AVO inversion by denoising the prestack gathers using curvelet and wavelet transforms. Li and Couzens (2006) design a time-frequency adaptive noise suppression to isolate and attenuate localized high-amplitude noise in prestack seismic data.

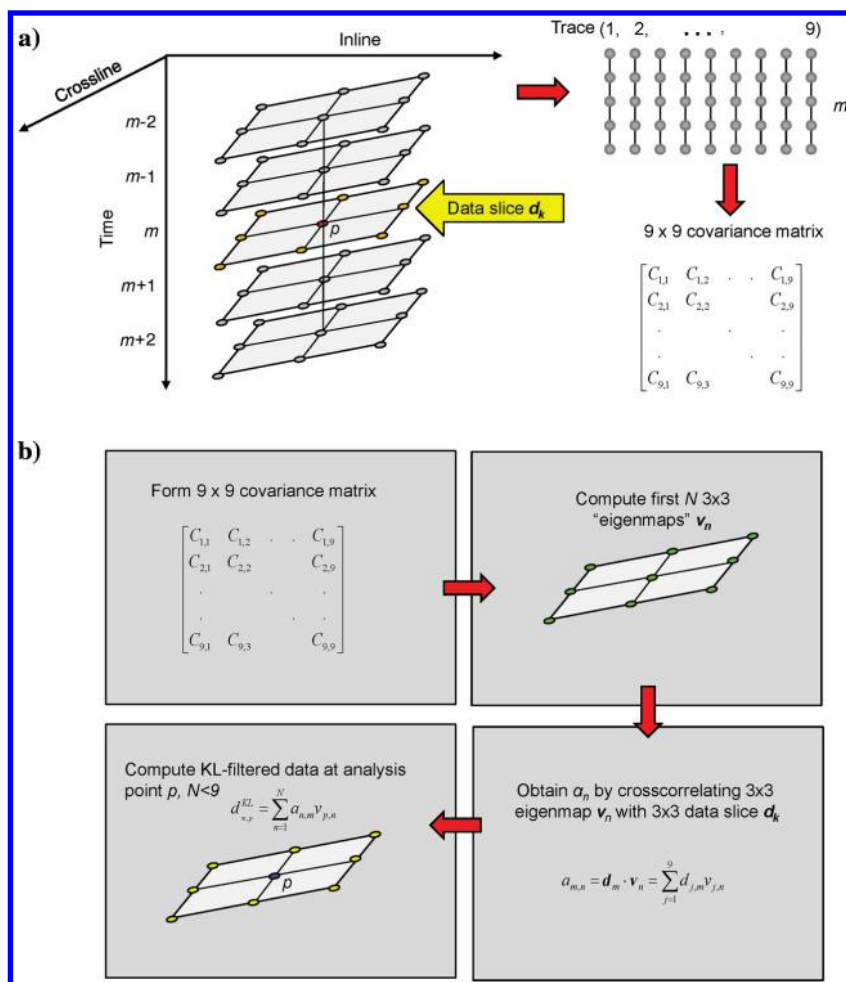


Figure 1. (a) Cartoon showing structure-oriented filtering applied to a post-stack data volume along the structural dip using a centered analysis window about the red analysis point. In this example, there are 3 crosslines \times 3 lines resulting in a length 9 sample vector for each interpolated dipping horizon slice at time k . These sample vectors are crosscorrelated and averaged from $k = -K$ to $k = +K$ ($K = 2$) time samples using equation 6 resulting in a 9×9 covariance matrix. (b) The first N length 9 eigenvectors represent 3 \times 3 maps that best represents the lateral variation of amplitude within the analysis window. These maps are crosscorrelated with the sample vector at time m to compute a suite of N principal components. One or more of these components are then summed to form the filtered data given by equation 9.

sion by applying it to a high fold seismic data volume acquired over the Fort Worth Basin (FWB), TX.

$$0 \leq \alpha \leq 0.5. \quad (5)$$

Methodology

Attenuation of noise and enhancement of structural continuity can significantly improve the quality of seismic interpretation and stabilize rock-property estimation by prestack analysis. As the name implies, the key steps for structure-oriented filtering are the accurate estimation of reflector dip followed by the application of a filter. In our application, we use a variation of the dip-scan estimation of reflector dip described by Marfurt (2006). Other accurate means of estimating reflector dip include the gradient structure tensor (as used by Fehmers and Höcker, 2003), “consistent dip” by crosscorrelating in a circuitous manner (Aarre et al., 2012), and plane-wave destructor methods that are similar to a lateral predictive deconvolution (Liu et al., 2010).

In terms of filtering, the more common methods include (1) mean filtering, (2) median filtering, (3) α -trimmed mean filtering, (4) LUM filtering, and (5) principal component (or KL) filtering. For the first four methods, the filters are based on length- J sample vectors oriented along a plane following reflector dip (Figure 1a). In this paper, d indicates the seismic amplitude. The mean filter is

$$d_m^{\text{mean}} = \frac{1}{J} \sum_{j=1}^J d_{j,m}, \quad (1)$$

where m is the time index and d_m^{mean} is the filtered output.

The next three filters require first sorting the data samples from low to high values: $\mathbf{u}_m = \text{sort}\{d_{1,m}, d_{2,m}, \dots, d_{J-1,m}, d_{J,m}\} = \{u_{1,m}, u_{2,m}, \dots, u_{J-1,m}, u_{J,m}\}$ such that $u_{1,m} \leq u_{2,m} \leq \dots \leq u_{J-1,m} \leq u_{J,m}$, where \mathbf{u}_m is the sorted amplitude values from low to high. The median filter is then

$$d_m^{\text{median}} = u_{(J+1)/2,m}, \quad (2)$$

where the α -trimmed mean filter is

$$d_m^{\alpha\text{-trim}} = \frac{1}{J - 2\alpha(J-1)} \sum_{j=1+\alpha(J-1)}^{J-\alpha(J-1)} u_{j,m}, \quad (3)$$

and the LUM filter is

$$d_m^{\text{LUM}} = \text{median}(u_{1+\alpha(J-1),m}, u_m^*, u_{J-\alpha(J-1),m}) = \begin{cases} u_{1+\alpha(J-1),m} & u_m^* < u_{1+\alpha(J-1),m} \\ u_{1-\alpha(J-1),m} & u_m^* > u_{1-\alpha(J-1),m} \\ u_m^* & \text{otherwise} \end{cases}, \quad (4)$$

where for the α -trimmed mean and LUM filters,

The principal component or KL filter has greater statistics that are computed from multiple sample vectors (again, planes for our application) above and below the analysis point p (Figure 1a and 1b). First, we form the covariance matrix

$$C_{i,j,m} = \frac{1}{2K+1} \sum_{k=-K}^{+K} (d_{i,m+k} - \omega_{i,m})(d_{j,m+k} - \omega_{j,m}), \quad (6)$$

where

$$\omega_{j,m} = \frac{1}{2K+1} \sum_{k=-K}^{+K} d_{j,m+k} \quad (7)$$

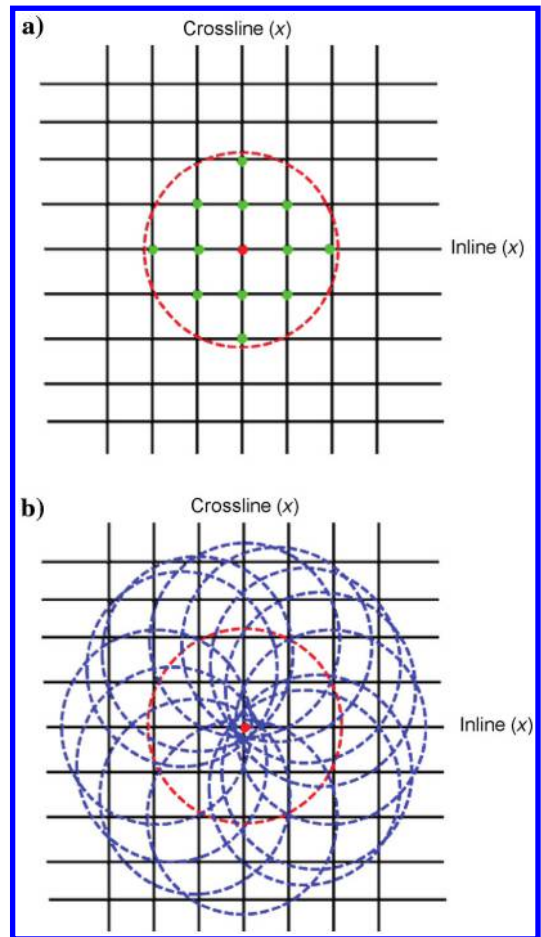


Figure 2. (a) A circular analysis window seen from above containing $J = 13$ seismic traces centered about the red analysis point. (b) The 13 overlapping Kuwahara windows, all of which contain the same red analysis point. In this workflow, coherence is computed within each window. The filter is then applied to the data window having the highest coherence, with the output being assigned to the (perhaps uncentered) red analysis point (after Davogustto, 2011).

is the local vertical mean within the analysis window of the j th trace, and K is the half-vertical window size along time axis. Given a suite of J traces ($J = 9$ in our example), the covariance matrix is defined as

$$C_m = \begin{bmatrix} C_{1,1,m} & C_{1,2,m} & \dots & C_{1,J,m} \\ C_{2,1,m} & C_{2,2,m} & & C_{2,J,m} \\ \vdots & & \ddots & \vdots \\ C_{J,1,m} & C_{J,2,m} & & C_{J,J,m} \end{bmatrix} \quad (8)$$

Figure 3. (a) Cartoon showing structure-oriented filtering applied to prestack common offset migrated gathers. The windows are oriented along structure and centered about the red analysis point. In this example, there are 3 CDPs \times 3 inlines and 3 offsets resulting in a length 27 sample vector for each interpolated horizon slice at time k . These sample vectors are crosscorrelated and averaged from $k = -K$ to $k = +K$ ($K = 2$) time samples using equation 6 resulting in a 27×27 covariance matrix. (b) As in Figure 1, the first length 27 eigenvectors represent three 3×3 maps, one for each of the three offsets. These maps are crosscorrelated with the sample vector at time k to compute a suite of N principal components. One or more of these components are then summed to form the filtered data.

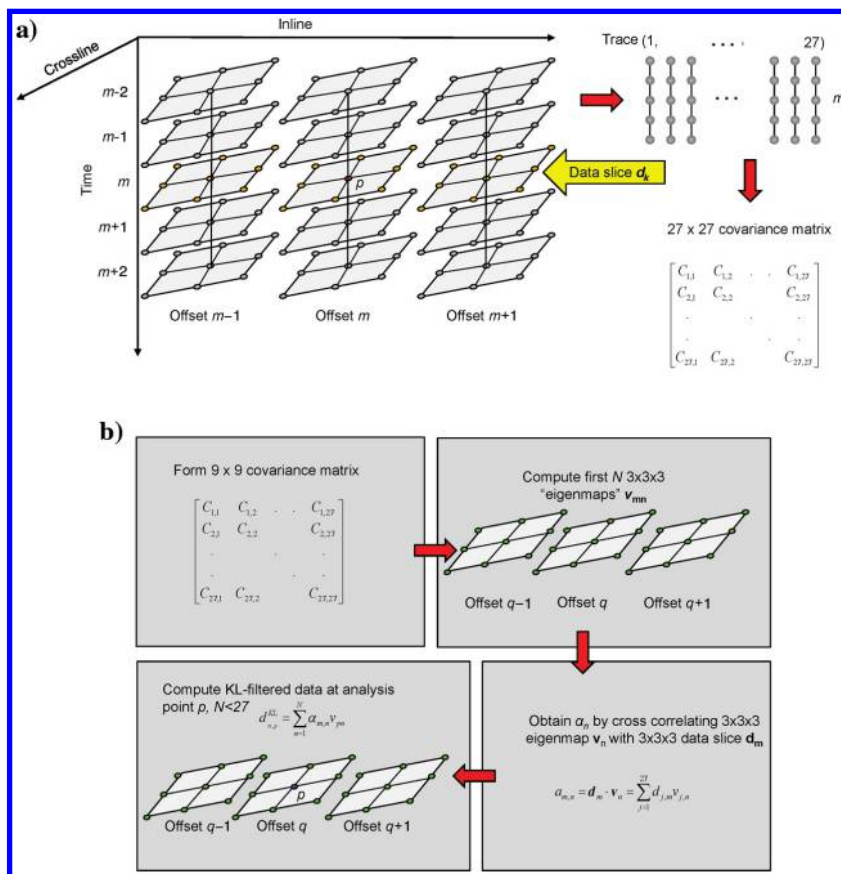
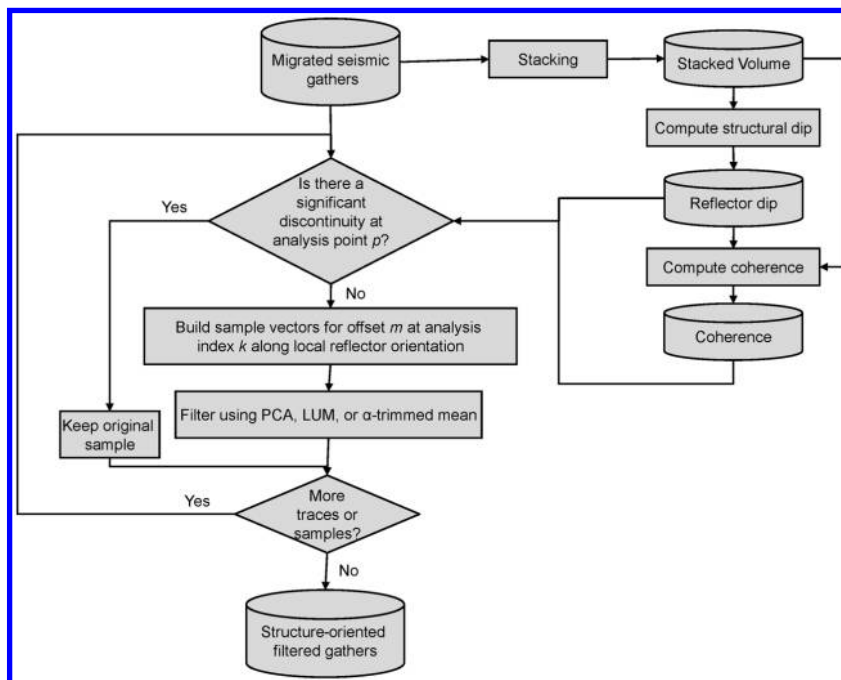


Figure 4. A simplified workflow of prestack-oriented filtering. The migrated data are stacked, which in turn provides an average estimate of structural dip and coherence. For each analysis point, one or more data points are extracted from either side along the structural dip in the adjacent inline direction, crossline direction, and offset direction, and if present, the azimuth direction to form a sample vector, such as that shown in Figure 3a. If the coherence falls below a lower threshold, a discontinuity is assumed to be present and no filtering is applied. If the coherence is above an upper threshold, the data are filtered using either a KL (principal component), LUM, or α -trimmed mean filter. In our actual implementation, we add a Kuwahara window construct (Marfurt, 2006), such that the filtering occurs in the most coherent (noncentered) window containing that analysis point.



The $J \times J$ covariance matrix \mathbf{C}_m is decomposed into J eigenvectors v_j and J eigenvalues λ_j , where by construction v_1 represents most of the lateral amplitude variation across the sample vectors. The v_2 best represents that part of the amplitude variation not represented by the eigenvector(s) before it, and so on. In general, seismic data aligned along a structurally oriented window are quite coherent, such that the first one or two eigenvectors represent the seismic reflection signal and the remaining eigenvectors represent less coherent noise. By construction, the eigenvectors have unit length. To compute the amplitude of the pattern represented by the n th eigenvector at time sample index m , we compute

$$a_{m,n} = \sum_{j=1}^J v_{j,n} d_{j,m} \quad (9)$$

and then reconstruct the signal (i.e., we KL filter the data) at the analysis point p

$$d_m^{\text{KL}} = \sum_{n=1}^N a_{n,m} v_{p,n}. \quad (10)$$

Principal component structure-oriented filtering can be quite effective in suppressing crosscutting migration operator aliasing and certain components of acquisition footprint on poststack data (Davogustto, 2011). Of the five filters presented, KL filtering best preserves signal amplitude when the noise is of low amplitude with approximately Gaussian statistics. However because the first eigenvectors represent the most energy in the data, KL filters behave poorly when the input data have high-amplitude spikes, in which case they represent the noise.

Figure 2a and 2b shows a plan view of the multi-window Kuwahara filter. The original analysis window

in Figure 2a represents a sample vector of length $J = 13$. In our implementation, we compute coherence (Gersztenkorn and Marfurt, 1999) in the 13 windows shown in Figure 2b, each of which contains the red analysis point p . Finally, one of the five filters described above is applied to the data falling within the window having the highest coherence, with filtered output being assigned to (a perhaps uncentered) analysis point.

In this paper, we apply a prestack structure-oriented filter (PSOF), which is based on the principal analysis (PCA), to the seismic gathers to improve the signal-to-noise ratio (S/N). Our algorithm is based on the following assumptions (1) coherent (i.e., non-Gaussian) noise, such as multiples and ground roll, has been previously filtered, (2) noise and reflected signals are uncorrelated and have zero mean, and (3) noise is uncorrelated from trace to trace and sample to sample in the gathers, that the first eigenvalue and eigenvector of covariance matrix of seismic traces corresponding to the reflection signals (Key and Smithson, 1990).

Figure 3a and 3b illustrates the steps for PSOF along local structure using a centered analysis window. We sort the prestack gathers into different common offset volumes and smooth the data along the local structure. In this example, there are 3 crosslines \times 3 inlines and 3 offsets resulting in a length 27 “sample vector” $\mathbf{d}_{j,m+k}$ ($j = 1, 2, \dots, 27$) for each interpolated horizon slice at time index m . These sample vectors are cross-correlated and averaged from $k = -K$ to $k = +K$ time samples using equation 6 resulting in a 27×27 covariance matrix. Similarly, we only extract the value of the analysis point (the red point in Figure 2b) from the “eigenmap.” Figure 4 summarizes the proposed workflow of PSOF by considering the geologic discontinuities. The workflow begins by stacking the original seismic gathers. We next estimate reflector orientation in a running window on all traces of the stacked volume (Marfurt, 2006). We then calculate the correlation coefficients for the stack volume along the local reflection

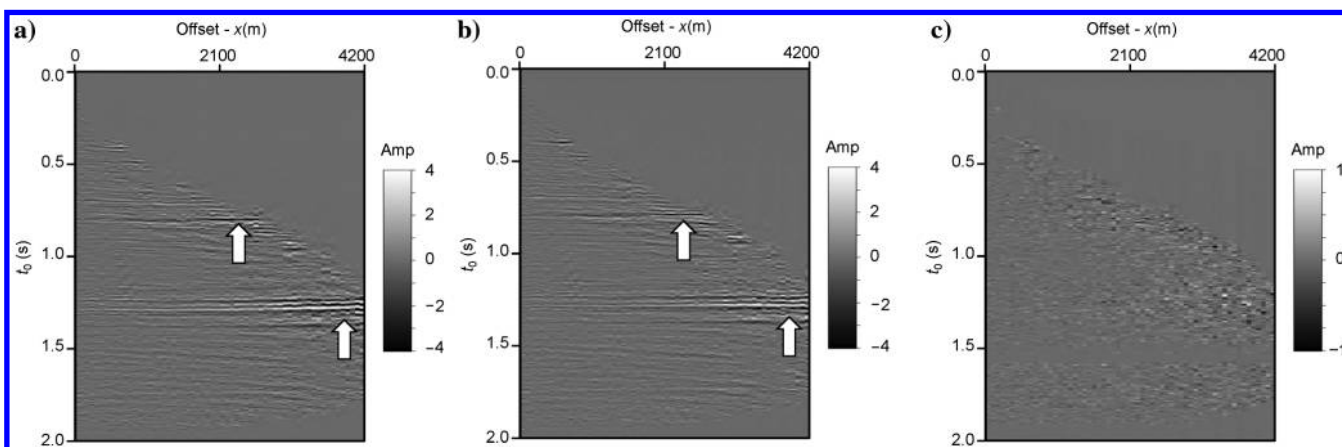


Figure 5. Representative gather with the conditioning workflow is shown in Figure 3. (a) The time-migrated gather after applying the nonstretch processing. (b) The same gather after applying prestack structure-oriented KL filtering. (c) The rejected noise. White arrows indicate noticeable improvements.

dip and azimuth (Gersztenkorn and Marfurt, 1999). To archive the edge preserving filtering, we only perform PCA filtering to those gathers, whose correlation coefficients are greater than a user-defined threshold through the first eigenvalue and eigenvector of seismic covariance matrix. The gathers whose correlation coefficients are less than the threshold are unchanged. In this manner, we improve the S/N and avoid smearing

the amplitude information across the geology discontinuities, such as faults and channel edges.

Application

To evaluate the effectiveness of our workflow, we first apply it to prestack time-migrated gathers acquired in the FWB, USA. We then compare the prestack inversion results based on unconditioned and conditioned gathers. The FWB is a foreland basin and covers approximately 14,000 km² (54,000 mi²) in north-central Texas (da Silva, 2013). The target is the Mississippian Barnett Shale, which is one of the largest unconventional reservoirs in the world and spreads approximately 72,520 km² (28,000 mi²) across the FWB. In our survey, the Barnett Shale Formation lies between 1.2 and 1.4 s, which is the “core” of the main production in the FWB. The maximum offset is approximately 4200 m, whereas the target Barnett Shale lies at approximately 2100 m depth.

Figure 5a shows a representative time-migrated CMP gather after nonstretch processing (Zhang et al., 2013). White arrows indicate the zone with obvious noise spikes. Figure 5b and 5c shows the same gather after PSOF was applied and the rejected noise, respectively. Note that the reflection events indicated by white arrows are clearer in the filtered gather. Figure 6a shows a stacked time slice through the target zone generated from unconditioned gathers (Figure 5a). Figure 6b and 6c shows the same stacked time slice after PSOF was applied and the rejected stacked noise. We do not observe much difference between Figure 6a and 6b due to the fact that the energy of the rejected noise is very small compared with that of the seismic signal. Note that stacking removes most of the random noise in the prestack gathers (Hendrickson, 1999). Figures 5c and 6c together indicate that PSOF removes random noise and artifacts introduced by acquisition or processing. Figure 7a and 7b shows the seismic well ties between stacked volumes and a well located in our study area. The procedure was done by correlating the stacked traces near the borehole with the synthetic seismogram generated from well logs. The correlation coefficient of conditioned seismic data (Figure 7a) is 0.835, whereas the coefficient of the unconditioned data (Figure 7b) is 0.818. We next extract the angle-dependent statistical wavelets for the unconditioned (Figure 8a) and the conditioned (Figure 8b) data after the seismic well tie. The red, blue, and green lines show the extracted small (0°–12°), intermediate (12°–24°), and large angle wavelets (24°–36°), respectively. We observe a slight improvement of large angle wavelets. To better compare the improvements, we show the amplitude spectrum of the extracted wavelets for unconditioned and conditioned gathers in Figure 8c and 8d. Note that the spectrum of the large angle wavelet is distorted for both cases. The narrower bandwidth of the large angle wavelets is due to a low-pass antialiasing filter applied to the far-offset data during the time migration processing (Biondi, 2001). However, we still no-

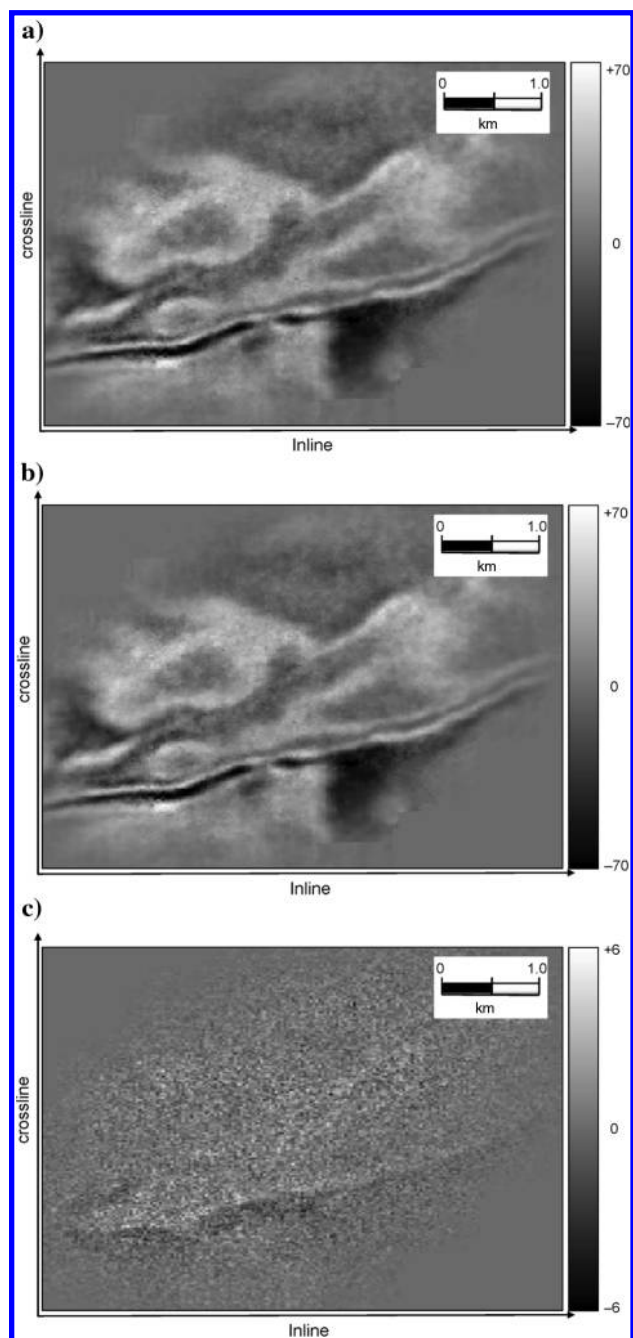


Figure 6. A stacked time slice through the target zone with the conditioning workflow in Figure 3. The time slice (a) before and (b) after applying prestack structure-oriented KL filtering. (c) The rejected noise. Note that while stacking removes most of the random noise, Figures 4c and 5c together indicate that the proposed workflow removes random noise and artifacts introduced by acquisition and processing.

tice a slight spectrum improvement for wavelets estimated from conditioned gathers.

The prestack inversion was conducted 50 ms above the top of Marble Falls limestone and 50 ms below the top of Viola limestone. Figures 9, 10, and 11 compare the inverted P-impedance, S-impedance, and density from unconditioned and conditioned gathers, respectively. We observe an overall improvement by rejecting the noise of prestack gathers. For example, the formations indicated by the white arrow are more laterally continuous in the new inverted sections when compared with those of unconditioned data. The zones in-

dicated by black arrows have higher resolution in the new inverted section when compared with that of conventional data. The faults indicated by the gray arrows are also easier to interpret in the new inverted sections. Note, the improvement of density is not as large as those of P- and S- impedance. This is due to the fact that the maximum incidence angle of our gather is approximately 36° and that it is beyond the capability to generate a reliable result. To better quantify the improvement, we quality control our inverted results from (Figure 12a) unconditioned and (Figure 12b) conditioned gathers with well logs at the target zone. Note, the new inverted

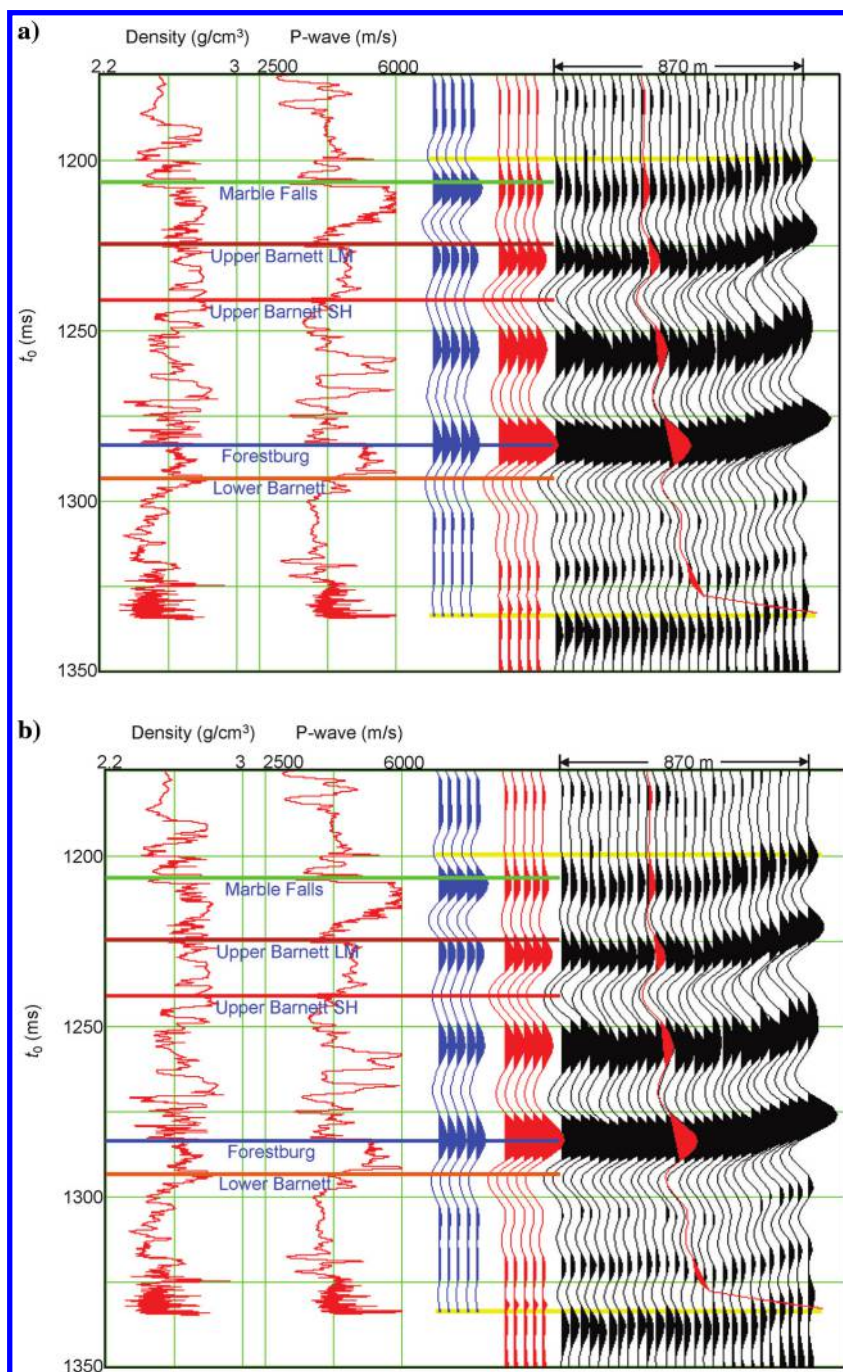


Figure 7. Seismic-well ties between (a) conditioned and (b) unconditioned stacked volume and a well located in our study area. The procedure was done by correlating the stacked traces nearby the borehole with the synthetic seismogram generated from well logs. We obtain the correlation coefficient of 0.835 for conditioned data and 0.818 for the unconditioned data.

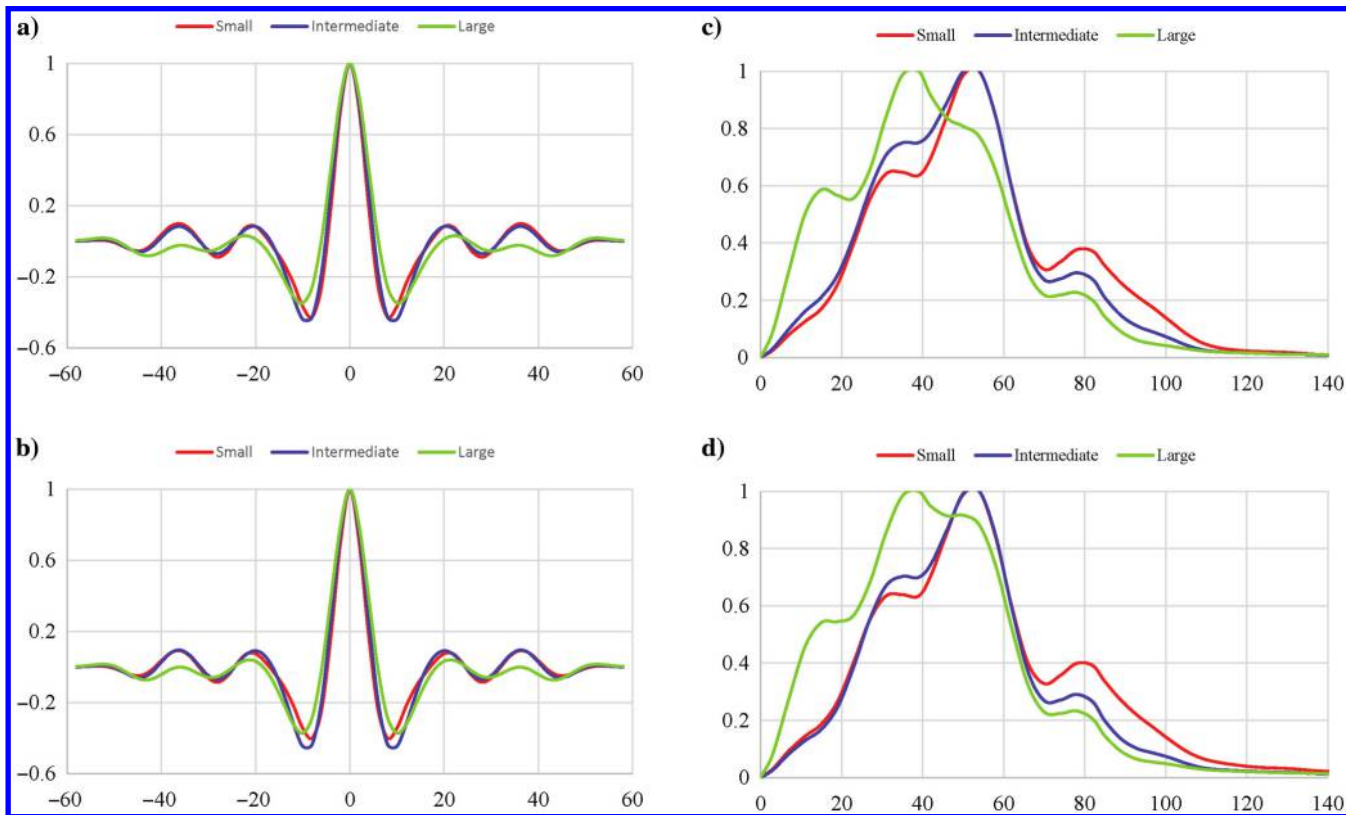
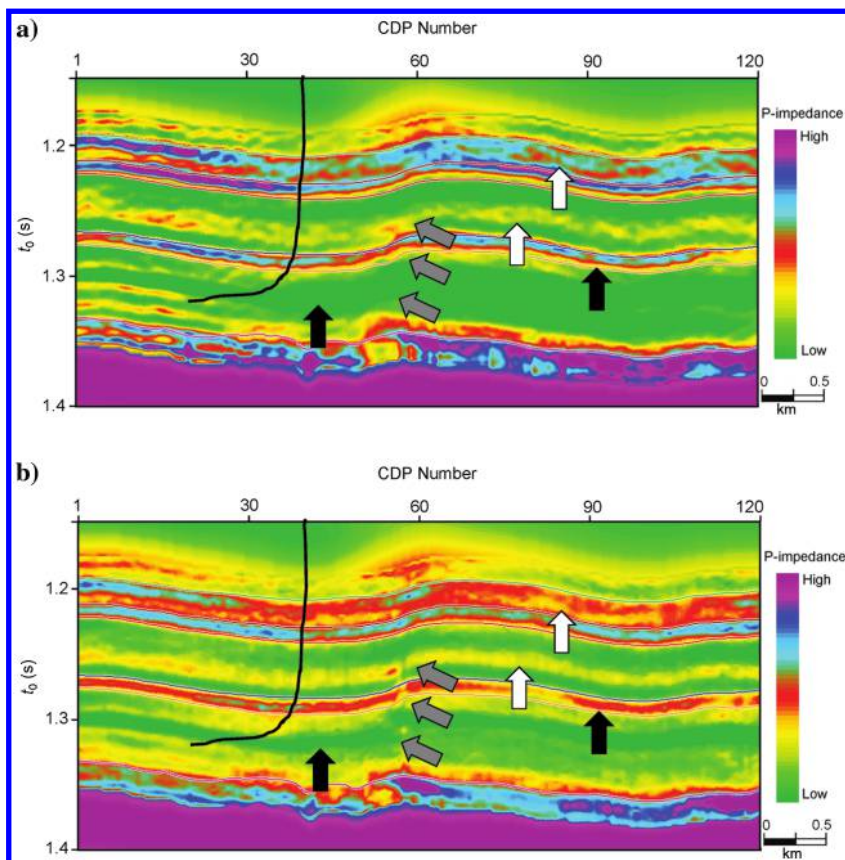


Figure 8. (a) Statistically extracted wavelets and corresponding amplitude spectra, (c and b) the unconditioned, and (d) conditioned angle gathers. The red, blue, and green curves corresponding to small, intermediate, and large angle wavelets. Note, the spectrum of the large angle wavelet is distorted to some extent; which is due to the application of an antialiasing filter in the Kirchhoff prestack migration algorithm. Nevertheless, we still notice a slight improvement of the wavelets after PSOF is applied.

Figure 9. Comparison of inverted P-impedance from (a) unconditioned and (b) conditioned gathers. White arrows indicate formations where we have more lateral continuity compared with the conventional data. The black arrows indicate the zones where we have higher resolution.



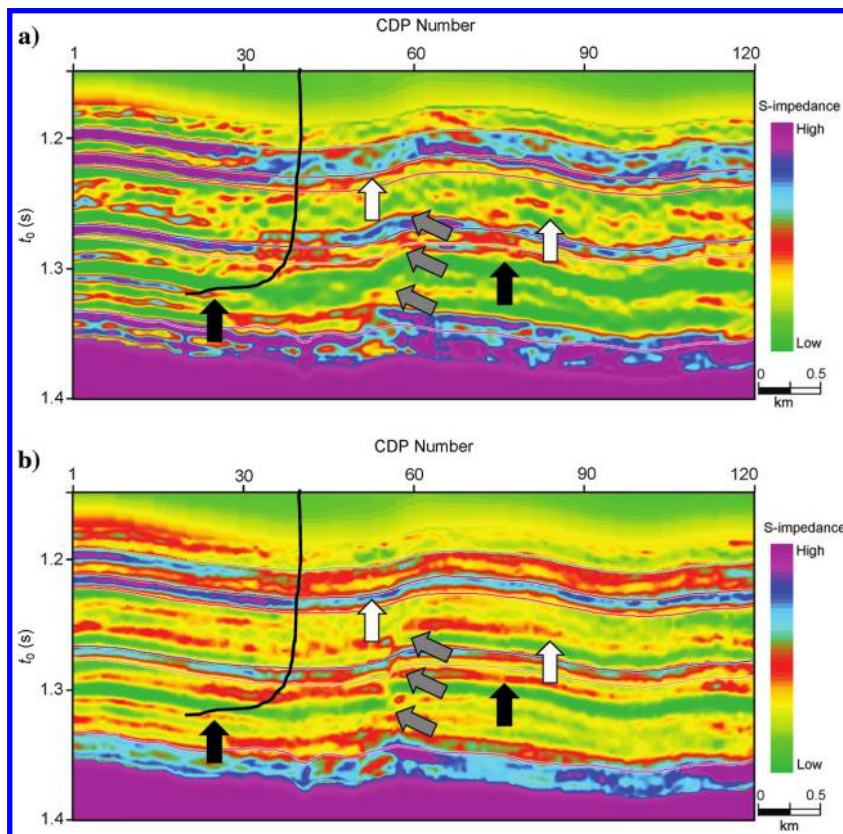


Figure 10. Comparison of inverted S-impedance form (a) unconditioned and (b) conditioned gathers. The white arrows indicate the formations, where we have more lateral continuity compared with that of conventional data. The black arrows indicate the zones where we have higher resolution.

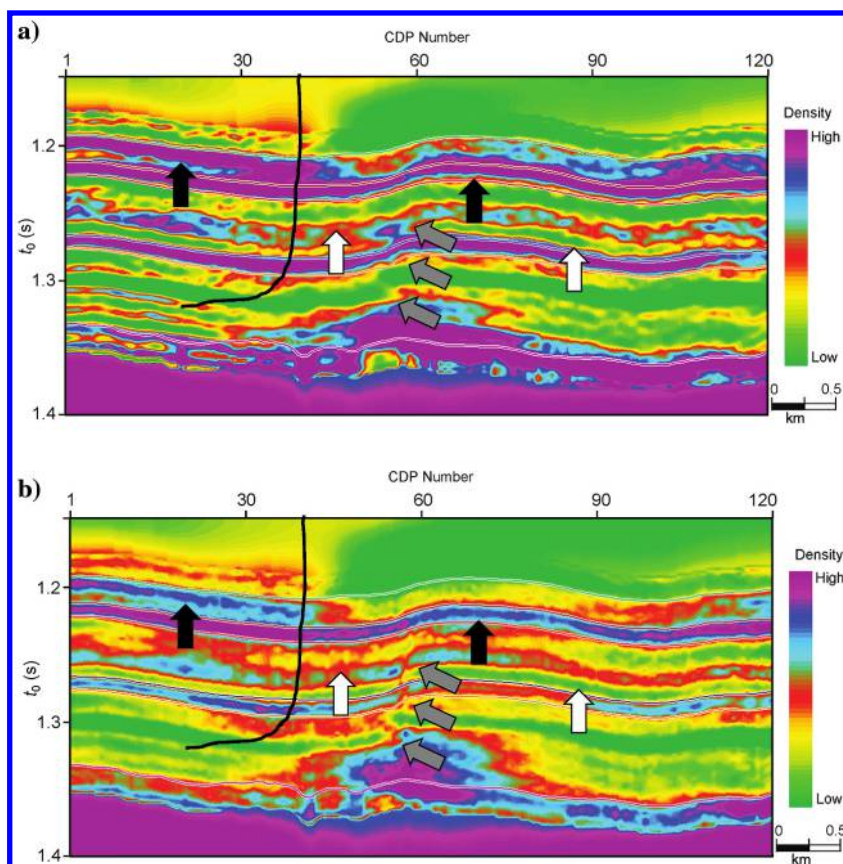


Figure 11. Comparison of inverted density form (a) unconditioned and (b) conditioned gathers. We did not observe any obvious improvement. Reliable density estimation requires the maximum incident angle of 45° , which is beyond that of our input data.

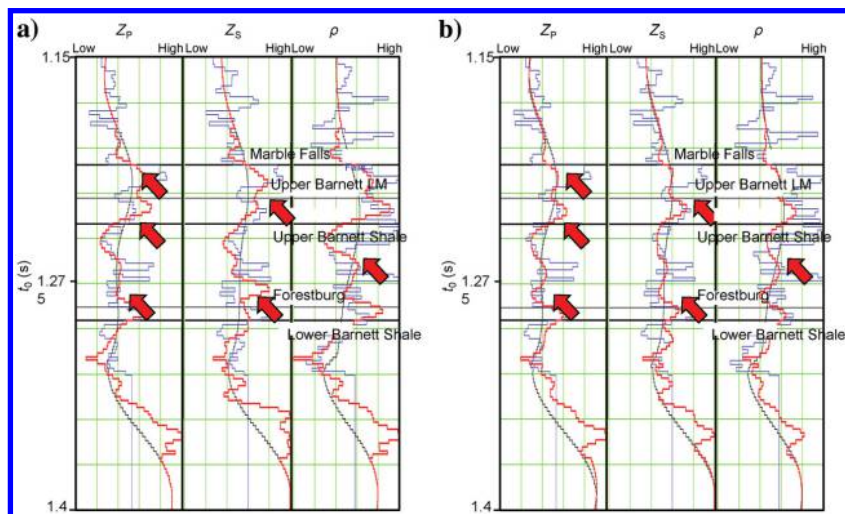


Figure 12. Validation of the inverted results with the original well logs. The left, middle, and right panels show the P-impedance, S-impedance, and density logs. The black, blue, and red curves show the original logs, initial model, and inverted results from conventional and new processing gathers. The red arrows indicate an obvious improvement zone.

results indicated by the red arrows have noticeable better correlation with original well logs and initial models, resulting lower inversion errors.

Conclusion

The proposed workflow not only removes random noise but also suppresses coherent acquisition, processing, and migration artifacts that crosscut the reflectors of interest. We preserve the edge information by only applying the algorithm to the prestack gathers whose coherency is larger than a user-defined threshold. Rejecting the noise in the prestack gathers results in (1) an improved stacked image, (2) a better seismic-well tie, (3) higher resolution and lateral continuities of inverted result, and (4) lower error between inverted elastic parameters and original well logs.

Acknowledgments

The authors would like to thank Devon Energy for providing the data and CGG for providing the license for Hampson-Russell. We also thank the financial support (PLC201401) from State Key Laboratory of Oil and Gas Reservoir Geology and Exploration, Chengdu University of Technology.

References

- Aarre, V., D. Astratti, T. N. A. Al Dayyani, S. L. Mahmoud, A. B. S. Clark, M. J. Stellas, J. W. Stringer, B. Toelle, O. V. Vejbaek, and G. White, 2012, Seismic detection of subtle faults and fractures: *Oilfield Review*, **24**, 28–43.
- AlBinHassan, N. M., Y. Luo, and M. N. Al-Faraj, 2006, 3-D edge-preserving smoothing and applications: *Geophysics*, **71**, no. 4, P5–P11, doi: [10.1190/1.2213050](https://doi.org/10.1190/1.2213050).
- Biondi, B., 2001, Kirchhoff imaging beyond aliasing: *Geophysics*, **66**, 654–666, doi: [10.1190/1.1444956](https://doi.org/10.1190/1.1444956).

- Buland, A., and H. Omre, 2003a, Bayesian linearized AVO inversion: *Geophysics*, **68**, 185–198, doi: [10.1190/1.1543206](https://doi.org/10.1190/1.1543206).
- Buland, A., and H. Omre, 2003b, Bayesian wavelet estimation from seismic and well data: *Geophysics*, **68**, 2000–2009, doi: [10.1190/1.1635053](https://doi.org/10.1190/1.1635053).
- Cambois, G., 1998, AVO attributes and noise-pitfalls of crossplotting: 68th Annual International Meeting, SEG, Expanded Abstracts, 244–247.
- Cambois, G., 2000, Can P-wave AVO be quantitative?: *The Leading Edge*, **19**, 1246–1251, doi: [10.1190/1.1438516](https://doi.org/10.1190/1.1438516).
- Castagna, J., and M. Backus, 1993, Offset-dependent reflectivity: Theory and practice of AVO analysis: SEG.
- Corrao, A., M. Fervari, and M. Galbiati, 2011, Hewett Plattendolomite: Reservoir characterization by resolution enhanced seismic data: GCSSEPM 31st Annual Bob F. Perkins Research Conference on Seismic Attributes — New Views on Seismic Imaging: Their Use in Exploration and Production, 66–99.
- da Silva, M., 2013, Production correlation to 3D seismic attributes in the Barnett Shale, Texas: M.S. thesis, The University of Oklahoma.
- Davogusto, E. O., 2011, Removing footprint from legacy seismic data volumes: M.S. thesis, The University of Oklahoma.
- Fehmers, G. C., and C. F. W. Höcker, 2003, Fast structural interpretation with structure-oriented filtering: *Geophysics*, **68**, 1286–1293, doi: [10.1190/1.1598121](https://doi.org/10.1190/1.1598121).
- Gersztenkorn, A., and K. J. Marfurt, 1999, Eigenstructure-based coherence computations as an aid to 3-D structural and stratigraphic mapping: *Geophysics*, **64**, 1468–1479, doi: [10.1190/1.1444651](https://doi.org/10.1190/1.1444651).
- Hale, D., 2011, Structure-oriented bilateral filtering of seismic images: 81st Annual International Meeting, SEG, Expanded Abstracts, 3596–3600.
- Helmre, S., 2009, Dealing with the noise — Improving seismic whitening and seismic inversion workflows using frequency split structurally oriented filters: 79th Annual International Meeting, SEG, Expanded Abstracts, 3367–3371.
- Hendrickson, J. S., 1999, Stacked: *Geophysical Prospecting*, **47**, 663–705, doi: [10.1046/j.1365-2478.1999.00150.x](https://doi.org/10.1046/j.1365-2478.1999.00150.x).
- Hennenfent, G., and F. Herrmann, 2004, Three-term amplitude-versus-offset (AVO) inversion revisited by curvelet and wavelet transforms: 74th Annual International Meeting, SEG, Expanded Abstracts, 211–214.
- Key, S., and S. B. Smithson, 1990, New approach to seismic-reflection event detection and velocity determination: *Geophysics*, **55**, 1057–1069, doi: [10.1190/1.1442918](https://doi.org/10.1190/1.1442918).
- Koza, S., and J. Castagna, 2003, The effects of noise on AVO crossplots: 73rd Annual International Meeting, SEG, Expanded Abstracts, 274–276.

- Li, X., and R. Couzens, 2006, Attacking localized high amplitude noise in seismic data — A method for AVO compliant noise attenuation: *CSEG Recorder*, **31**, 32–36.
- Liu, Y., S. Fomel, and G. Liu, 2010, Nonlinear structure-enhancing filtering using plane-wave prediction: *Geophysical Prospecting*, **58**, 415–427, doi: [10.1111/\(ISSN\)1365-2478](https://doi.org/10.1111/(ISSN)1365-2478).
- Luo, Y., S. Al-Dossary, and M. Alfaraj, 2002, Edge-preserving smoothing and applications: *The Leading Edge*, **21**, 136–158, doi: [10.1190/1.1452603](https://doi.org/10.1190/1.1452603).
- Marfurt, K. J., 2006, Robust estimates of 3D reflector dip and azimuth: *Geophysics*, **71**, no. 4, P29–P40, doi: [10.1190/1.2213049](https://doi.org/10.1190/1.2213049).
- Simm, R., R. White, and R. Uden, 2000, The anatomy of AVO crossplots: *The Leading Edge*, **19**, 150–155, doi: [10.1190/1.1438557](https://doi.org/10.1190/1.1438557).
- Singleton, S., 2008, The effects of seismic data conditioning on pre-stack simultaneous impedance inversion: 78th Annual International Meeting, SEG, Expanded Abstracts, 1506–1510.
- Tomasi, C., and R. Manduchi, 1998, Bilateral filtering for gray and color images: *Proceedings of the 6th International Conference on Computer Vision*, IEEE Computer Society, 839.
- Wang, J., Y. Chen, D. Xu, and Y. Qiao, 2009, Structure-oriented edge-preserving smoothing based on accurate estimation of orientation and edges: *Applied Geophysics*, **6**, 367–376, doi: [10.1007/s11770-009-0038-6](https://doi.org/10.1007/s11770-009-0038-6).
- Weickert, J., 1999, Coherence-enhancing diffusion filtering: *International Journal of Computer Vision*, **31**, 111–127, doi: [10.1023/A:1008009714131](https://doi.org/10.1023/A:1008009714131).
- Whitcombe, D. N., L. Hodgson, H. Hoerber, and Z. Yu, 2008, Frequency dependent, structurally conformable filtering: 78th Annual International Meeting, SEG, Expanded Abstracts, 2617–2621.
- Zhang, B., K. Zhang, S. Guo, and K. J. Marfurt, 2013, Non-stretching NMO correction of prestack time-migrated gathers using a matching-pursuit algorithm: *Geophysics*, **78**, no. 1, U9–U18, doi: [10.1190/geo2011-0509.1](https://doi.org/10.1190/geo2011-0509.1).



Bo Zhang received a B.S. (2002) at China University of Petroleum (Hua-dong) and master degree (2006) at the Institute of Geology and Geophysics, Chinese Academy of Sciences in geophysics. In 2009, he joined an industry-supported consortium (AASPI) at the University of Oklahoma as a Ph.D. student in geophysics. In 2014,

he joined the Michigan Technological University as a visiting assistant professor. In 2015, he joined the University of Alabama as an assistant professor. His current research interests include broadband seismic data processing, development and calibration of new seismic attributes, pattern recognition of geologic features on 3D seismic data, and shale resource play characterization.



Shiguang Guo received a master's degree in geophysics and a Ph.D. in geophysics from the University of Oklahoma. The topic of the Ph.D degree consists of three areas, which are 5D interpolation, preconditioned least-squares prestack time migration and vector correlation between azimuthal anisotropy, and curvature for fractures prediction of unconventional resources. Now he serves as geophysicist at Schlumberger. His research interests include developing new methods for seismic interpretation and processing, especially fractures prediction and anisotropy modeling for rock physics.



Kurt J. Marfurt joined The University of Oklahoma in 2007 where he serves as the Frank and Henrietta Schultz Professor of Geophysics within the ConocoPhillips School of Geology and Geophysics. Marfurt's primary research interest is in the development and calibration of new seismic attributes to aid in seismic processing, seismic interpretation, and reservoir characterization. Recent work has focused on applying coherence, spectral decomposition, structure-oriented filtering, and volumetric curvature to mapping fractures and karst with a particular focus on resource plays. Marfurt earned a Ph.D. in applied geophysics at Columbia University's Henry Krumb School of Mines in New York in 1978 where he also taught as an Assistant Professor for four years. He worked 18 years in a wide range of research projects at Amoco's Tulsa Research Center after which he joined the University of Houston for 8 years as a Professor of Geophysics and the Director of the Allied Geophysics Lab. In addition to teaching and research duties at OU, Marfurt leads short courses on attributes for the SEG and AAPG.

Biographies and photographs of the other authors are not available.